Progress In Electromagnetics Research, PIER 85, 211–226, 2008

ANALYSIS AND CORRECTION OF BOREHOLE EFFECT ON THE RESPONSES OF MULTICOMPONENT INDUCTION LOGGING TOOLS

X. Sun and Z. Nie

School of Electronic Engineering
University of Electronic Science and Technology of China
Chengdu 610054, China

A. Li and X. Luo

China Oilfield Service Limited
Beijing 101149, China

Abstract—The analytical formulae based on the generalized reflection and transmission coefficient matrices for cylindrically stratified media are used to simulate the borehole effect on multicomponent induction logging responses in various ratios of mud conductivity and formation conductivity and to investigate the tool's eccentricity effect on the responses of coplanar coils and coaxial coils. The simulated data show that the borehole effect and the tool's eccentricity effect on the response of coplanar coils is greater than that on the response of coaxial coils in most cases. Then we give an algorithm for the correction of borehole effect on multicomponent induction logging responses, and the algorithm is based on the above-mentioned formulae to build forward model and regularized Newton method. Finally we correct borehole effect on the apparent conductivity responses of two different models with the algorithm, and the results demonstrate the effectiveness of the algorithm.

1. INTRODUCTION

There is about 30 percent hydrocarbon in thinly laminated sand and shale reservoir rocks which is electrically anisotropic for macro-resistivity in estimation. The electromagnetic induction logging method is among the most important methods to evaluate the water and hydrocarbon saturation in shaly sand formation. Conventional

induction logging tools comprising the axial direction component of transmitter and receiver can only provide coaxial measurements, which only yield horizontal resistivity for a vertical well or some weighted value of vertical resistivity and horizontal resistivity for a deviated or horizontal well. However, for thinly laminated sand and shale reservoir rocks, whose individual beds are beyond the resolution limits of conventional induction tools, the macro-resistivity is anisotropic, and a multicomponent electromagnetic induction logging tool has been developed to try to simultaneously evaluate the horizontal and vertical resistivity of the earth formations [1–3]. In addition to the coaxial transmitter-receiver pair, the new tool has two mutually orthogonal coplanar transmitter-receiver pairs, so theoretically it can provide nine components of magnetic field produced by the three mutually orthogonal transmitters. Therefore, the multicomponent electromagnetic induction measurement can resolve the anisotropic resistivity of earth formations.

In general, finite difference method [4–6] and finite element method [7–10, 23, 24] are employed for three-dimensional numerical modeling of the new tools. However the three-dimensional numerical simulation is time-consuming and inefficient. Electromagnetic modeling by using Green's function for layered media is a fast method to compute the field excited by dot source of any direction in layered media [11–17]. Based on the generalized reflection and transmission coefficient matrices for cylindrically stratified media, Wang [18] deduced the Green's function for cylindrically stratified anisotropic media, and mainly investigated the multicomponent induction logging responses for various lengths of tools. We use the Green's function to quickly compute the borehole effect and eccentricity effect on multicomponent induction logging responses in various ratios of mud conductivity and formation conductivity, and make use of it to build forward model in borehole correction algorithm.

Usually a correction algorithm is used to reduce or to eliminate the borehole effect and eccentricity effect on multicomponent induction logging. The borehole correction algorithm consists of building forward model to compute coil responses and using iterative inversion method to solve some of the borehole effect parameters. A table is usually built as a forward model by using three-dimensional numerical methods such as finite difference method [19]. However, building the table with the three-dimensional numerical method is very time-consuming. We thus build the forward model with the above-mentioned analytical formulae. So the correction algorithm is accurate and efficient to correct borehole effect.

2. THE FIELD EXCITED BY THE DOT SOURCE IN CYLINDRICALLY STRATIFIED ANISOTROPIC MEDIA

A well model usually includes borehole mud, invasion and a formation, when the formation is homogeneous in the axial direction, as shown in Fig. 1 where Region 1 is the borehole, Region 2 the invasion and Region 3 the formation. If we suppose that the conductivity of the formation is uniaxially anisotropic, then $\bar{\sigma}$ can be expressed as:

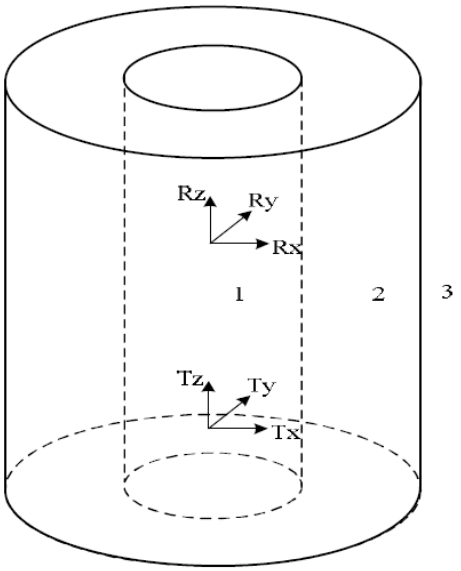

Figure 1. Model of multicomponent induction logging tool in cylindrically stratified anisotropic formation.

$$\bar{\sigma} = \begin{bmatrix} \sigma_H & & \\ & \sigma_H & \\ & & \sigma_V \end{bmatrix} \tag{1}$$

where $\sigma_{H,V}$ is the horizontal and vertical conductivity respectively.

When a dot source of any direction is placed in Region j, the field in Region j can be represented as [17, 18]

$$\begin{pmatrix} H_{j,z} \\ E_{j,z} \end{pmatrix} = \int_{-\infty}^{+\infty} dk_z \left\{ \sum_{n=-\infty}^{\infty} e^{in(\varphi-\varphi_s)} e^{ik_z|z-z_s|} \begin{pmatrix} \tilde{H}_{j,nz} \\ \tilde{E}_{j,nz} \end{pmatrix} \right\} \tag{2}$$

$$\begin{pmatrix} E_{j,\rho} \\ E_{j,\theta} \end{pmatrix} = \int_{-\infty}^{+\infty} dk_z \left\{ \sum_{n=-\infty}^{+\infty} e^{in(\theta-\theta_s)} \begin{pmatrix} \frac{i\omega\mu}{\rho\left(k_{\rho j}^h\right)^2}\frac{\partial}{\partial\theta} & \frac{ik_z}{\lambda_{ej}^2\left(k_{\rho j}^e\right)^2}\frac{\partial}{\partial\rho} \\ \frac{-i\omega\mu}{\left(k_{\rho j}^h\right)^2}\frac{\partial}{\partial\rho} & \frac{ik_z}{\lambda_{ej}^2\left(k_{\rho j}^e\right)^2\rho}\frac{\partial}{\partial\rho} \end{pmatrix} \begin{pmatrix} \tilde{H}_{j,nz} \\ \tilde{E}_{j,nz} \end{pmatrix} \right\} \tag{3}$$

$$\begin{pmatrix} H_{j,\rho} \\ H_{j,\theta} \end{pmatrix} = \int_{-\infty}^{+\infty} dk_z \left\{ \sum_{n=-\infty}^{+\infty} e^{in(\theta-\theta_s)} \begin{pmatrix} \frac{ik_z}{\left(k_{\rho j}^h\right)^2}\frac{\partial}{\partial\rho} & \frac{\sigma_{hj}}{\lambda_{ej}^2\left(k_{\rho j}^e\right)^2\rho}\frac{\partial}{\partial\theta} \\ \frac{ik_z}{\left(k_{\rho j}^h\right)^2\rho}\frac{\partial}{\partial\theta} & \frac{-\sigma_{hj}}{\lambda_{ej}^2\left(k_{\rho j}^e\right)^2}\frac{\partial}{\partial\rho} \end{pmatrix} \begin{pmatrix} \tilde{H}_{j,nz} \\ \tilde{E}_{j,nz} \end{pmatrix} \right\} \tag{4}$$

where

$$\begin{aligned} \begin{pmatrix} \tilde{H}_{j,nz} \\ \tilde{E}_{j,nz} \end{pmatrix} &= (\bar{\mathbf{J}}_n^{(1)}(\mathbf{k}_{j,\rho}\rho_<)\bar{\mathbf{H}}_n^{(1)}(\mathbf{k}_{j,\rho}\rho_>) + \bar{\mathbf{J}}_n^{(1)}(\mathbf{k}_{j,\rho}\rho)\boldsymbol{b}_{j,n} \\ &\quad + \bar{\mathbf{H}}_n^{(1)}(\mathbf{k}_{j,\rho}\rho)\boldsymbol{a}_{j,n}) \cdot \overleftarrow{\mathbf{D}}_{0,\mathrm{n}} \end{aligned} \tag{5}$$

$$\bar{\mathbf{J}}_n(\mathbf{k}_{j,\rho}\rho) = \begin{bmatrix} J_n(k_{j,\rho}^h\rho)\ 0 \\ 0\ J_n(k_{j,\rho}^e\rho) \end{bmatrix},\ \bar{\mathbf{H}}_n^{(1)}(\mathbf{k}_{j,\rho}\rho) = \begin{bmatrix} H_n^{(1)}(k_{j,\rho}^h\rho)\ 0 \\ 0\ H_n^{(1)}(k_{j,\rho}^e\rho) \end{bmatrix} \tag{6}$$

$$\begin{aligned} \boldsymbol{a}_{j,n} &= (\mathbf{I} - \tilde{\bar{\mathbf{R}}}_{n,j,j-1}\tilde{\bar{\mathbf{R}}}_{n,j,j+1})^{-1}\tilde{\bar{\mathbf{R}}}_{n,j,j-1} \\ &\quad \left(\bar{\mathbf{H}}_n^{(1)}(\mathbf{k}_{j,\rho}\rho_s) + \tilde{\bar{\mathbf{R}}}_{n,j,j+1}\bar{\mathbf{J}}_n(\mathbf{k}_{j,\rho}\rho_s)\right) \\ \boldsymbol{b}_{j,n} &= (\mathbf{I} - \tilde{\bar{\mathbf{R}}}_{n,j,j+1}\tilde{\bar{\mathbf{R}}}_{n,j,j-1})^{-1}\tilde{\bar{\mathbf{R}}}_{n,j,j+1} \\ &\quad \left(\bar{\mathbf{J}}_n(\mathbf{k}_{j,\rho}\rho_s) + \tilde{\bar{\mathbf{R}}}_{n,j,j-1}\bar{\mathbf{H}}_n^{(1)}(\mathbf{k}_{j,\rho}\rho_s)\right) \end{aligned} \tag{7}$$

where $J_n(k_{j,\rho}^h\rho)$ and $H_n^{(1)}(k_{j,\rho}^h\rho)$ are the n-order of Bessel function and n-order of Hankel function of the first kind, $k_z = \sqrt{i\omega u_0\sigma_V}$ is the axial direction wave number, $k_{j,\rho}^h = \sqrt{i\omega u_{0,j}\sigma_{h,j} - k_z^2}$ and $k_{j,\rho}^h = \sqrt{i\omega u_{0,j}\sigma_{H,j} - k_z^2\frac{\sigma_{V,j}}{\sigma_{H,j}}}$ are the radial direction wave numbers of TE and TM waves in layer j respectively, and the $\overleftarrow{\mathbf{D}}_{0,\mathrm{n}}$ operator, the local reflection and transmission coefficient matrices and generalized reflection matrix are expressed in appendix.

As for the induction logging problem, the source is usually in Region 1 as shown in Fig. 1. So the field in the source region can be written as [17, 18]

$$\begin{pmatrix} \tilde{H}_{j,nz} \\ \tilde{E}_{j,nz} \end{pmatrix} = \left(\bar{\mathbf{J}}_n(\mathbf{k}_{1,\rho}\rho_<)\bar{\mathbf{H}}_n^{(1)}(\mathbf{k}_{1,\rho}\rho_>) + \bar{\mathbf{J}}_n(\mathbf{k}_{1,\rho}\rho)\tilde{\bar{\mathbf{R}}}_{n,1,2}\bar{\mathbf{J}}_n(\mathbf{k}_{1,\rho}\rho_s)\right)\overleftarrow{\mathbf{D}}_{0,\mathrm{n}} \tag{8}$$

3. CORRECTING THE BOREHOLE EFFECT

In this section, we develop a technique for correcting the borehole effect. The borehole correction algorithm consists of building forward model to compute array responses in the two-layered cylindrically stratified model and using iterative inversion method to solve some of the borehole effect parameters. We build the forward model with the above-mentioned analytical formulae (1)–(3), and use regularized Newton method as the inversion method. Flow chart of algorithm for correcting the borehole effect is shown in Fig. 2.

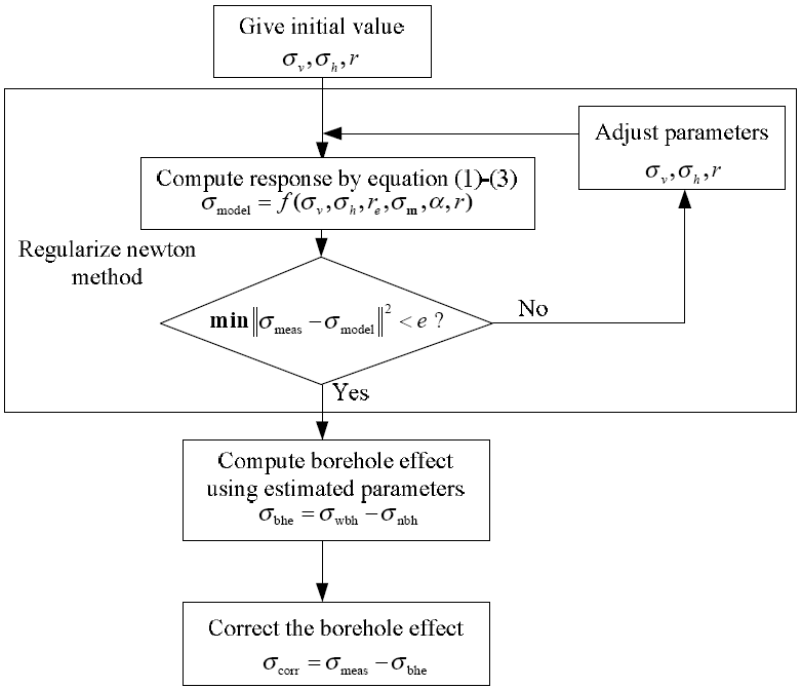

Figure 2. Flow chart of algorithm for correcting borehole effect.

Because borehole effect mainly depends on the six parameters [19]: the borehole radius r, the borehole mud conductivity σ_m, the offset r_e, the offset direction relative to the tool coordinate α, the formation vertical conductivity σ_v, the formation horizontal conductivity σ_h. The parameters r, σ_m are easy to get by measurement, and the direction of the offset with respect to the tool's x-axis can be solved directly from

the xz and xy couplings. The relation is given by the equation [19]

$$\alpha = -\arctan\left(\frac{\sigma_{yz}}{\sigma_{xz}}\right) \tag{9}$$

The residual three parameters r_e, σ_v, σ_h are solved by the inversion method. There are many inversion methods [20–22] to solve the minimization problem. In this paper, the regularized Newton method [3, 20] is used to minimize the penalty function C.

$$C(\sigma_h, \sigma_v, r_e) = \|\sigma_{meas} - \sigma_{model}\,(\sigma_h, \sigma_v, r_e, \sigma_m, r, \alpha)\|^2 \tag{10}$$

The algorithm of the regularized Newton method is described by Zhdanov [3], if n is the iteration index

$$\begin{aligned} \boldsymbol{r}_n &= f(\boldsymbol{m}_n) - \boldsymbol{d} \\ \boldsymbol{I}_n &= \boldsymbol{F}^T \boldsymbol{r}_n + v_n(\boldsymbol{m}_n - \boldsymbol{m}_{apr}) \\ \boldsymbol{H}_n &= \boldsymbol{F}^T \boldsymbol{F} + v_n \boldsymbol{I} \\ \boldsymbol{m}_{n+1} &= \boldsymbol{m}_n - \boldsymbol{H}_n^{-1} \boldsymbol{I}_n \end{aligned} \tag{11}$$

where $f(\cdot)$ is the operator of the forward modeling described by formulae (2)–(4), $\boldsymbol{d}$ is a vector of observed data, $\boldsymbol{m}_n$ is a vector of model parameters (horizontal and vertical conductivity, σ_v and σ_h, and the offset) on the n-th iteration, $\boldsymbol{m}_{apr}$ is a priori model, $\boldsymbol{r}_n$ is a residual vector of the difference between the predicted $f(\boldsymbol{m}_n)$ and observed data $\boldsymbol{d}$ on the n-th iteration, $\boldsymbol{F}$ is a Frechet derivative matrix, $\boldsymbol{H}_n$ is a quasi Hessian matrix, $\boldsymbol{I}_n$ is the regularized direction of a Newton method on the n-th iteration, and v_n is the regularization parameter that is updated on each iteration according to a progression of the number.

$$\begin{aligned} v_0 &= \frac{\|f(\boldsymbol{m}_1) - \boldsymbol{d}\|^2}{\|\boldsymbol{m}_1 - \boldsymbol{m}_{apr}\|^2} \\ v_n &= v_0 q^n,\ 0 < q < 1 \end{aligned} \tag{12}$$

The Frechet derivative matrix can be calculated by taking derivatives $f(\boldsymbol{m}_m)$, with respect to unknown parameters. The matrix is

$$\boldsymbol{F} = \frac{\partial f}{\partial \boldsymbol{m}} \tag{13}$$

When six parameters are got by the above-mentioned method, we can compute the borehole effect σ_{bhe} with the equation

$$\sigma_{\mathrm{bhe}} = \sigma_{\mathrm{wbh}} - \sigma_{\mathrm{nbh}} \tag{14}$$

where σ_{wbh} is the response of the model with the estimated parameters, and σ_{nbh} is the response of the model without borehole. σ_{wbh} and σ_{nbh} can be computed with the formulae (1)–(3). Finally, the corrected response can be solved by

$$\sigma_{\text{corr}} = \sigma_{\text{meas}} - \sigma_{\text{bhe}} \tag{15}$$

4. NUMERICAL RESULTS

In this section, we first investigate the borehole effect and tool's eccentricity effect on multicomponent induction logging responses with formulae (1)–(3), and then correct the borehole effect with the above-mentioned correction algorithm method. The basic structure of multicomponent induction tool is shown in Fig. 3. T_x, T_y and T_z are the three mutually orthogonal transmitter coils; R_x, R_y and R_z are the three mutually orthogonal receiver coils.

4.1. Borehole Effect

Assuming a centralized tool, the borehole effect depends on formation conductivity, mud conductivity and borehole radius. To investigate different borehole effects on responses of coplanar coils and on that of coaxial coils, we compute the ratios of $\sigma_{xx}/\sigma^0_{xx}$ and $\sigma_{zz}/\sigma^0_{zz}$ for various contrasts σ_m/σ_f, where σ^0_{xx} and σ^0_{zz} are the apparent vertical and horizontal conductivities without a borehole respectively, σ_{xx} and σ_{zz} are the apparent vertical and horizontal conductivities with a borehole respectively, σ_m and σ_f are the mud conductivity and formation

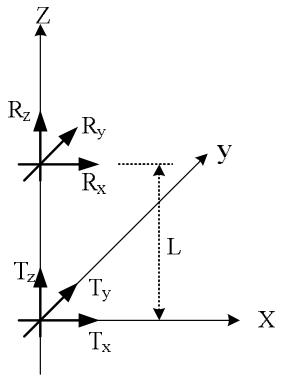

Figure 3. Illustration of the basic structure of multicomponent induction logging tool.

conductivity respectively. The borehole radius is assumed to be 0.1 m. The distance R1 between the main receiver and the transmitter is 1.4 m. The distance R2 between the buck receiver and the transmitter is 0.8 m. Fig. 4 shows $\sigma_{xx}/\sigma^0_{xx}$ and $\sigma_{zz}/\sigma^0_{zz}$ as functions of σ_m/σ_f for 4 different formation conductivities $\sigma_f = 0.01,\ 0.05,\ 0.1,\ 0.5$ S/m. We observe that when the σ_m/σ_f is less than 100, σ_{zz} is slightly affected

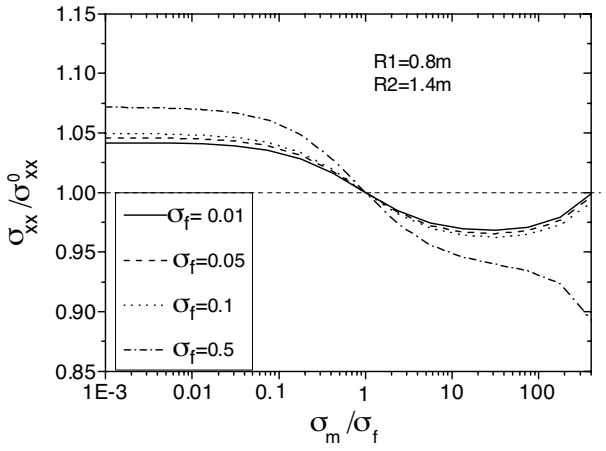

(a) Responses of coplanar coils

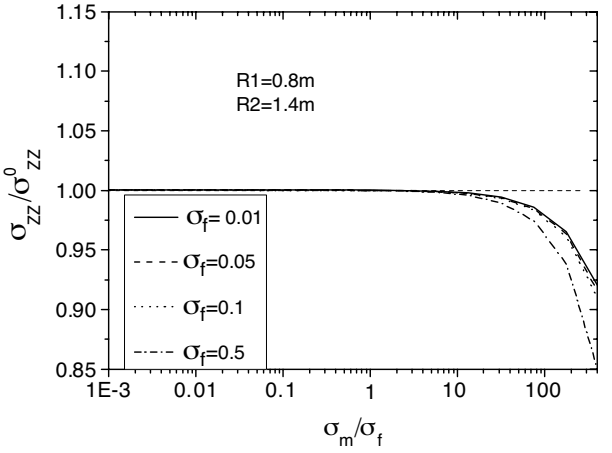

(b) Responses of coaxial coils

Figure 4. Borehole effect, expressed as $\sigma_{xx}/\sigma^0_{xx}$ (a) and $\sigma_{zz}/\sigma^0_{zz}$ (b) as functions of σ_m/σ_f for 4 different conductivities $\sigma_f = 0.01, 0.05, 0.1, 0.5$.

by borehole mud. However, σ_{xx} is affected by all types of borehole mud. When the formation conductivity is greater than 0.5 S/m, the borehole effect become greater for the same σ_m/σ_f ratio.

4.2. Eccentricity Effect

In a deviated well, tool weight prevents the tool from being centralized. The decentralized tool will increase the influence of response. We simulate the tool eccentricity effect for different axial offsets. The borehole radius to be assumed is 0.15 m. The tool is decentralized in

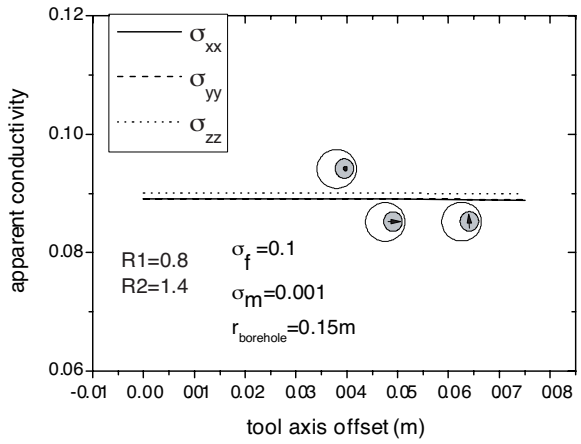

(a) Resistive mud

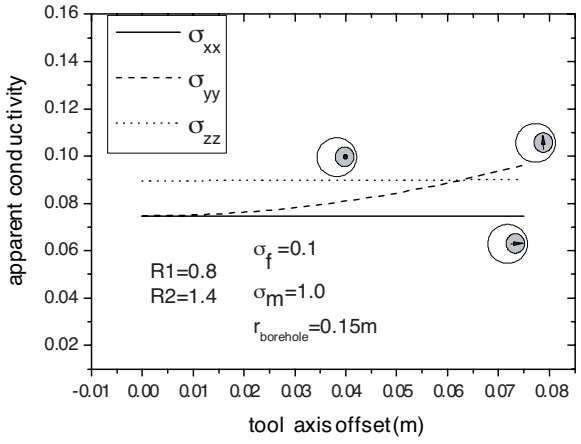

(b) Conductive mud

Figure 5. Tool's eccentricity effect for different tool axis offsets.

the x-direction. The formation conductivity is 0.1 S/m. The distance R1 between the main receiver and the transmitter is 1.4 m. The distance R2 between the buck receiver and the transmitter is 0.8 m. We consider both the resistive (oil base 0.001 S/m) mud and the conductive (water base 1.0 S/m) mud. Fig. 5(a) and Fig. 5(b) show the eccentricity effect for resistive mud and conductivity mud respectively. We observe that the eccentricity effect on all responses is little for resistive mud. However, the eccentricity effect on σ_{yy} is great, and the eccentricity effect on σ_{xx} and σ_{zz} is little for conductive mud.

4.3. Correction of Borehole Effect

We have known that borehole effect on the coplanar coils is greater than that on the coaxial coils. To illustrate the effectiveness of the above-mentioned method of correcting borehole effect, we compute the apparent conductivity response of the homogeneous formation with borehole. The conductivity of formation is 0.05 S/m, and the conductivity of borehole mud is 1.0 S/m. Then we correct borehole effect on apparent conductivities σ_{xx} and σ_{zz}, as shown in Fig. 6. We can observe that the apparent vertical conductivity σ_{xx} without borehole correction is quite different from the true formation conductivity. The apparent horizontal conductivity σ_{zz} is also unequal to the true formation conductivity. However, the apparent vertical and horizontal conductivities with correction are in accordance with the true formation conductivity.

We also try to correct the borehole effect on multicomponent induction logging response in a three-layered formation with borehole.

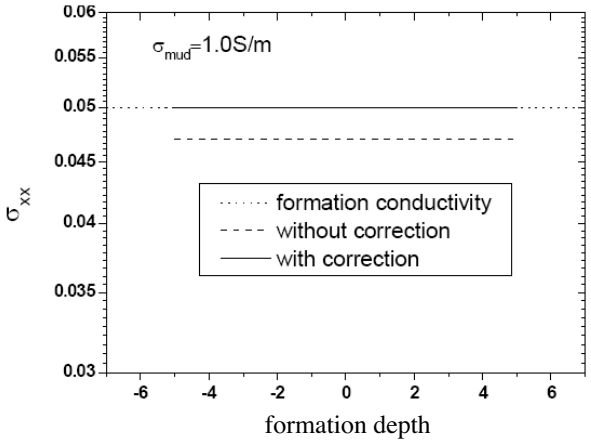

(a) Apparent vertical conductivity

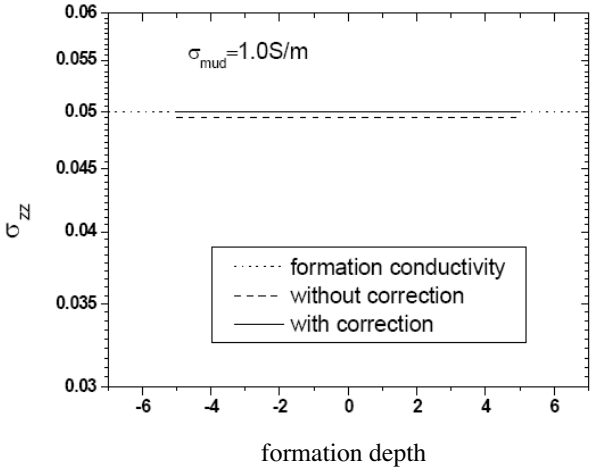

(b) Apparent horizontal conductivity

Figure 6. Comparison of apparent conductivity responses of homogeneous formation with borehole both with and without borehole correction.

The upper and lower layers have isotropic conductivity $\sigma_h = \sigma_v = 0.2\,\mathrm{s/m}$, whereas the middle layer has anisotropic conductivity $\sigma_h = 0.05\,\mathrm{s/m}$, $\sigma_v = 0.01\,\mathrm{s/m}$. The middle bed is 15 m thick. The borehole has a radius of 0.1 m. We compute the response of forward model by

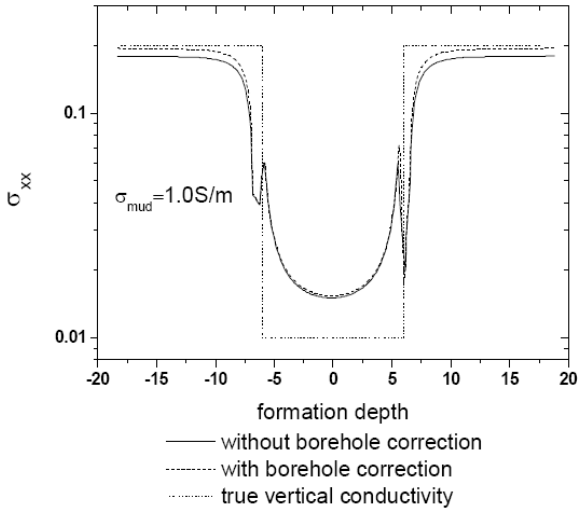

(a) Apparent vertical conductivity

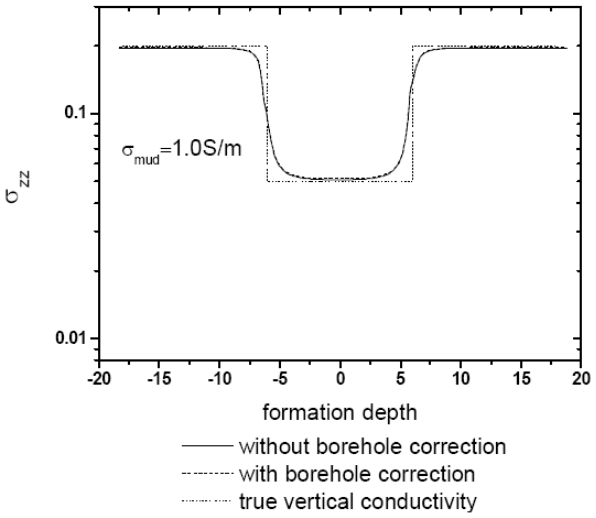

(b) Apparent horizontal conductivity

Figure 7. Comparison of apparent conductivities both with and without borehole correction.

finite element method [7, 8], then correct the borehole effect on the response of three-layered model with the above-mentioned correction algorithm. Fig. 7 illustrates the comparison of apparent conductivities σ^a_{xx}, σ^a_{yy} both with and without borehole correction. The results show that the apparent conductivities with borehole correction are more close to the formation's true conductivity than that without borehole correction.

5. CONCLUSION

We have given the analytical formulae to compute the field excited by magnetic dipole in any direction in cylindrically stratified anisotropic media, and then computed the borehole effect and tool's eccentricity effect on multicomponent induction logging response in different borehole environment with the analytical formulae, and we observe that the apparent vertical conductivity is affected more greatly by borehole mud for an σ_m/σ_f ratio up to about 100 than the apparent horizontal conductivity. The apparent vertical conductivity is affected by all types of mud. Eccentricity effect on all responses is slight for resistive mud. However, the eccentricity effect on the response of coplanar coils in the direction vertical to eccentricity direction

is great for conductive mud. We also give a algorithm to correct the borehole effect on multicomponent induction logging responses, and the numerical results illustrate that the algorithm can effectively correct the borehole effect.

APPENDIX A.

The $\overleftarrow{\mathbf{D}}_{0,\mathrm{n}}$ operator shown in function (7) can be expressed as [17, 18]

$$\overleftarrow{\mathbf{D}}_{0,\mathrm{n}} = \frac{1}{8\pi} \begin{pmatrix} -k_z \frac{\partial}{\partial \rho_s} & \frac{ink_z}{\rho_s} & -i\left(k_\rho^h\right)^2 \\ -\frac{in\omega\mu_h}{\rho_s} & -\omega\mu_h \frac{\partial}{\partial \rho_s} & 0 \end{pmatrix} \begin{pmatrix} M_\rho \\ M_\theta \\ M_z \end{pmatrix} \tag{A1}$$

where M_ρ, M_θ and M_z are the three orthonormal components of the magnetic dipole M in cylindrical coordinate system.

The local reflection and transmission coefficient matrices for cylindrically stratified uniaxial anisotropic media can be written as [17, 18]

$$\begin{aligned}
\bar{\mathbf{R}}_{n,j,j+1} &= -[\bar{\mathbf{B}}_{j,n}\bar{\mathbf{J}}_n(\mathbf{k}_{j,\rho}a_{j+1}) - \bar{\mathbf{B}}_{j+1,n}\bar{\mathbf{H}}_n^{(1)}(\mathbf{k}_{j+1,\rho}a_{j+1}) \\
&\quad \cdot(\bar{\mathbf{H}}_n^{(1)}(\mathbf{k}_{j+1,\rho}a))^{-1}\bar{\mathbf{J}}_n(\mathbf{k}_{j,\rho}a_{j+1})]^{-1} \\
&\quad [\bar{\mathbf{B}}_{j,n}\bar{\mathbf{H}}_n^{(1)}(\mathbf{k}_{j,\rho}a_{j+1}) - \bar{\mathbf{B}}_{j+1,n}\bar{\mathbf{H}}_n^{(1)}(\mathbf{k}_{j+1,\rho}a_{j+1}) \\
&\quad \cdot(\bar{\mathbf{H}}_n^{(1)}(\mathbf{k}_{j+1,\rho}a_{j+1}))^{-1}\bar{\mathbf{H}}_n^{(1)}(\mathbf{k}_{j,\rho}a_{j+1})] \\
\bar{\mathbf{T}}_{n,j,j+1} &= -[\bar{\mathbf{B}}_{j+1,n}\bar{\mathbf{H}}_n^{(1)}(\mathbf{k}_{j+1,\rho}a_{j+1}) - \bar{\mathbf{B}}_{j,n}\bar{\mathbf{J}}_n(\mathbf{k}_{j,\rho}a_{j+1}) \\
&\quad \cdot(\bar{\mathbf{J}}_n(\mathbf{k}_{j,\rho}a))^{-1}\bar{\mathbf{H}}_n^{(1)}(\mathbf{k}_{j+1,\rho}a_{j+1})]^{-1} \\
&\quad [\bar{\mathbf{B}}_{j,n}\bar{\mathbf{H}}_n^{(1)}(\mathbf{k}_{j,\rho}a_{j+1}) - \bar{\mathbf{B}}_{j+1,n}\bar{\mathbf{J}}_n(\mathbf{k}_{j,\rho}a_{j+1}) \\
&\quad \cdot(\bar{\mathbf{J}}_n(\mathbf{k}_{j,\rho}a_{j+1}))^{-1}\bar{\mathbf{H}}_n^{(1)}(\mathbf{k}_{j,\rho}a_{j+1})] \\
\bar{\mathbf{R}}_{n,j,j-1} &= -[\bar{\mathbf{B}}_{j,n}\bar{\mathbf{H}}_n^{(1)}(\mathbf{k}_{j,\rho}a_j) - \bar{\mathbf{B}}_{j-1,n}\bar{\mathbf{J}}_n(\mathbf{k}_{j-1,\rho}a_j) \\
&\quad \cdot(\bar{\mathbf{J}}_n(\mathbf{k}_{j-1,\rho}a_j))^{-1}\bar{\mathbf{H}}_n^{(1)}(\mathbf{k}_{j,\rho}a_j)]^{-1} \\
&\quad [\bar{\mathbf{B}}_{j,n}\bar{\mathbf{J}}_n(\mathbf{k}_{j,\rho}a_j) - \bar{\mathbf{B}}_{j-1,n}\bar{\mathbf{J}}_n(\mathbf{k}_{j-1,\rho}a_j) \\
&\quad \cdot(\bar{\mathbf{J}}_n(\mathbf{k}_{j-1,\rho}a_j))^{-1}\bar{\mathbf{J}}_n(\mathbf{k}_{j,\rho}a_j)] \\
\bar{\mathbf{T}}_{n,j,j-1} &= -[\bar{\mathbf{B}}_{j-1,n}\bar{\mathbf{J}}_n(\mathbf{k}_{j-1,\rho}a_j) - \bar{\mathbf{B}}_{j,n}\bar{\mathbf{H}}_n^{(1)}(\mathbf{k}_{j,\rho}a_j) \\
&\quad \cdot(\bar{\mathbf{H}}_n^{(1)}(\mathbf{k}_{j,\rho}a_j))^{-1}\bar{\mathbf{J}}_n(\mathbf{k}_{j-1,\rho}a)]^{-1} \\
&\quad [\bar{\mathbf{B}}_{j,n}\bar{\mathbf{J}}_n(\mathbf{k}_{j,\rho}a_j) - \bar{\mathbf{B}}_{j+1,n}\bar{\mathbf{H}}_n^{(1)}(\mathbf{k}_{j,\rho}a_j) \\
&\quad \cdot(\bar{\mathbf{H}}_n^{(1)}(\mathbf{k}_{j,\rho}a_j))^{-1}\bar{\mathbf{J}}_n(\mathbf{k}_{j,\rho}a_j)]
\end{aligned} \tag{A2}$$

where

$$\bar{\mathbf{B}}_{j,n} = \begin{pmatrix} -\frac{nk_z}{\lambda_{mj}^2 \left(k_{j\rho}^h\right)^2 \rho} & \frac{i\omega\varepsilon}{\lambda^2 \left(k_{j\rho}^e\right)^2} \frac{\partial}{\partial\rho} \\ -\frac{i\omega\mu_j}{\left(k_{j\rho}^h\right)^2} \frac{\partial}{\partial\rho} & \frac{-nk_z}{\lambda^2 \left(k_{j\rho}^e\right)^2} \frac{1}{\rho} \end{pmatrix} \tag{A3}$$

The generalized reflection coefficient matrix can be expressed as

$$\begin{aligned} \tilde{\bar{\mathbf{R}}}_{n,j,j+1} &= \bar{\mathbf{R}}_{n,j,j+1} + \bar{\mathbf{T}}_{n,j+1,j} \tilde{\bar{\mathbf{R}}}_{n,j+1,j+2} \left(\bar{\mathbf{I}} - \bar{\mathbf{R}}_{n,j+1,j} \tilde{\bar{\mathbf{R}}}_{n,j+1,j+2}\right)^{-1} \\ &\quad \cdot \bar{\mathbf{T}}_{n,j,j+1} \\ \tilde{\bar{\mathbf{R}}}_{n,j+1,j} &= \bar{\mathbf{R}}_{n,j+1,j} + \bar{\mathbf{T}}_{n,j,j+1} \tilde{\bar{\mathbf{R}}}_{n,j,j-1} \left(\bar{\mathbf{I}} - \bar{\mathbf{R}}_{n,j,j+1} \tilde{\bar{\mathbf{R}}}_{n,j,j-1}\right)^{-1} \bar{\mathbf{T}}_{n,j+1,j} \end{aligned} \tag{A4}$$

where $j = 1, 2, \ldots, J$, and $\bar{\mathbf{R}}_{n,J,J+1} = 0$, $\bar{\mathbf{R}}_{n,1,0} = 0$.

REFERENCES

1. Kriegshauser, B., O. Fanini, S. Forgang, G. Itskovich, M. Rabinovich, L. Tabarovsky, L. Yu, M. Epov, et al., "A new multicomponent induction loggingtool to resolve anisotropic formations," *SPWLA 40th Ann. Log. Symp.*, paper D., 2000.
2. Zhdanov, M. S., D. Kennedy, and E. Peksen, "Foundation of the tensor induction well logging," *Perophysics*, Vol. 42, No. 6, 588–610, 2001.
3. Zhdanov, M. S., W. D. Kennedy, A. B. Cheryauka, and E. Peksen, "Principles of tensor induction well logging in a deviated well in an anisotropic medium," *SPWLA 42th Ann. Log. Symp.*, June 17–20, 2001.
4. Wang, T., L. Yu, and F. Otto, "Multicomponent induction response in a borehole environment," *Geophysics*, Vol. 68, No. 5, 1510–1518, 2003.
5. Wang, T. and S. Fang, "3-D electromagnetic anisotropy modeling using finite differences," *Geophysics*, Vol. 66, No. 6, 1386–1398, 2001.
6. Shen, J. S., "Modeling of the multi-component induction log in anisotropic medium by using finite difference method," *Progress In Geophysics of China*, Vol. 19, No. 1, 101–107, 2004.
7. Sun, X. Y. and Z. P. Nie, "Vector finite element analysis of multicomponent induction response in anisotropic formations," *Progress In Electromagnetics Research*, PIER 81, 21–39, 2008.

8. Sun, X. Y., Z. P. Nie, A. Y. Li, and L. Xi, "Numerical modeling of multicomponent induction response in planar layered anisotropic formation," *Chinese Geophysics*, submitted for publication.
9. Shen, J. S., "Modeling of the 3-D electromagnetic responses to the anisotropic medium by the edge finite element method," *Well Logging Technology of China*, Vol. 28, 11–15, Feb. 2004.
10. Everett, M. E., E. A. Badea, L. C. Shen, G. A. Merchant, and C. J. Weiss, "3-D finite element analysis of induction logging in a dipping formation," *IEEE Trans. Geoscience and Remote Sensing*, Vol. 39, 2244–2252, October 2003.
11. Michalski, K. A. and J. R. Mosing, "Multilayered media Green's functions in integral formulations," *IEEE Trans. on Antennas and Propagation*, Vol. 45, No. 3, 508–519, 1997.
12. Svezhentsev, A. Y., "Mixed-potential Green's function of an axially symmetric sheet magnetic current on a circular cylindrical metal surface," *Progress In Electromagnetics Research*, PIER 60, 245–264, 2006.
13. Eroglu, A. and J. K. Lee, "Dyadic Green's functions for an electrically gyrotropic medium," *Progress In Electromagnetics Research*, PIER 58, 223–241, 2006.
14. Sun, J., C.-F. Wang, L.-W. Li, and M.-S. Leong, "Mixed potential spatial domain Green's functions in fast computational form for cylindrically stratified media," *Progress In Electromagnetics Research*, PIER 45, 181–199, 2004.
15. Li, L.-W., N.-H. Lim, W.-Y. Yin, and J.-A. Kong, "Eigenfunctional expansion of dyadic Green's functions in gyrotropic media using cylindrical vector wave functions," *Progress In Electromagnetics Research*, PIER 43, 101–121, 2003.
16. Gao, G., C. Torres-Verdin, and T. M. Habashy, "Analytical techniques to evaluate the integrals of 3d and 2d spatial dyadic Green's functions," *Progress In Electromagnetics Research*, PIER 52, 47–80, 2005.
17. Chew, W. C., *Waves and Fields in Inhomogeneous Media*, Van Nostrand Reinhold, New York, 1990.
18. Wang, H., P. So, S. Yang, and W. J. R. Hoefer, "Numerical modeling of multicomponent induction well-logging tools in the cylindrically stratified anisotropic media," *IEEE Trans. Geoscience and Remote Sensing*, Vol. 46, No. 4, 1134–1147, April 2008.
19. Barber, T., B. Anderson, and A. Abubakar, "Determining formation resistivity anisotropy in the presence of invasion," *SPE*

Annual Technical Conference and Exhibition Held in Houston, Texas, U.S.A., September 2004.

20. Habashy, T. M. and A. Abubakar, "A general framework for constraint minimization for the inversion of electromagnetic measurements," *Progress In Electromagnetics Research*, PIER 46, 265–312, 2004.
21. Avdeev, D. B. and A. D. Avdeeva, "A rigorous three-dimensional magnetotelluric inversion," *Progress In Electromagnetics Research*, PIER 62, 41–48, 2006.
22. Abubakar, A., T. M. Habashy, and P. M. Van den Berg, "Nonlinear inversion of multi-frequency microwave fresnel data using the multiplicative regularized contrast source inversion," *Progress In Electromagnetics Research*, PIER 62, 193–201, 2006.
23. Pingenot, J., "Full wave analysis of signal attenuation in a lossy rough surface cave using a high order time domain vector finite element method," *Journal of Electromagnetic Waves and Applications*, Vol. 20, No. 12, 1695–1705, 2006.
24. Hernandez-Lopez, M. A. and M. Quintillan-Gonzalez, "A finite element method code to analyse waveguide dispersion," *Journal of Electromagnetic Waves and Applications*, Vol. 21, No. 3, 397–408, 2007.